The Astrophysical Journal Letters, 979:L21 (14pp), 2025 February 1 https://doi.org/10.3847/2041-8213/ad9ddc

A Repeating Fast Radio Burst Source in the Outskirts of a Quiescent Galaxy

Vishwangi Shah[1,2], Kaitlyn Shin[3,4], Calvin Leung[5,27], Wen-fai Fong[6,7], Tarraneh Eftekhari[6,27], Mandana Amiri[8], Bridget C. Andersen[1,2], Shion Andrew[3,4], Mohit Bhardwaj[9], Charanjot Brar[10], Tomas Cassanelli[11], Shami Chatterjee[12], Alice Curtin[1,2], Matt Dobbs[1,2], Yuxin Dong (董雨欣)[6,7], Fengqiu Adam Dong[8], Emmanuel Fonseca[13,14], B. M. Gaensler[15,16,17], Mark Halpern[8], Jason W. T. Hessels[1,2,18,19], Adaeze L. Ibik[16,17], Naman Jain[1,2], Ronniy C. Joseph[1,2], Jane Kaczmarek[20], Lordrick A. Kahinga[15], Victoria M. Kaspi[1,2], Bikash Kharel[13,14], Tom Landecker[21], Adam E. Lanman[3,4], Mattias Lazda[16,17], Robert Main[1], Lluis Mas-Ribas[15], Kiyoshi W. Masui[3,4], Ryan Mckinven[1,2], Juan Mena-Parra[16,17], Bradley W. Meyers[22], Daniele Michilli[3,4], Kenzie Nimmo[3], Ayush Pandhi[16,17], Swarali Shivraj Patil[13,14], Aaron B. Pearlman[1,2,28], Ziggy Pleunis[18,19], J. Xavier Prochaska[15,23,24], Masoud Rafiei-Ravandi[1], Mawson Sammons[1,2], Ketan R. Sand[1,2], Paul Scholz[17,25], Kendrick Smith[26], and Ingrid Stairs[8]

[1] Department of Physics, McGill University, 3600 rue University, Montréal, QC H3A 2T8, Canada; vishwangi.shah@mail.mcgill.ca
[2] Trottier Space Institute, McGill University, 3550 rue University, Montréal, QC H3A 2A7, Canada
[3] MIT Kavli Institute for Astrophysics and Space Research, Massachusetts Institute of Technology, 77 Massachusetts Ave, Cambridge, MA 02139, USA
[4] Department of Physics, Massachusetts Institute of Technology,77 Massachusetts Avenue, Cambridge, MA 02139, USA
[5] Department of Astronomy, University of California, Berkeley, CA 94720, USA
[6] Center for Interdisciplinary Exploration and Research in Astronomy (CIERA), Northwestern University, 1800 Sherman Avenue, Evanston, IL 60201, USA
[7] Department of Physics and Astronomy, Northwestern University, Evanston, IL 60208, USA
[8] Department of Physics and Astronomy, University of British Columbia, 6224 Agricultural Road, Vancouver, BC V6T 1Z1, Canada
[9] McWilliams Center for Cosmology & Astrophysics, Department of Physics, Carnegie Mellon University, Pittsburgh, PA 15213, USA
[10] NRC Herzberg Astronomy and Astrophysics, 5071 West Saanich Road, Victoria, BC V9E2E7, Canada
[11] Department of Electrical Engineering,Universidad de Chile, AvenueTupper 2007, Santiago 8370451, Chile
[12] Cornell Center for Astrophysics and Planetary Science, Cornell University, Ithaca, NY 14853, USA
[13] Department of Physics and Astronomy, West Virginia University, P.O. Box 6315, Morgantown, WV 26506, USA
[14] Center for Gravitational Waves and Cosmology, West Virginia University, Chestnut Ridge Research Building, Morgantown, WV 26505, USA
[15] Department of Astronomy and Astrophysics, University of California Santa Cruz, 1156 High Street, Santa Cruz, CA 95064, USA
[16] David A. Dunlap Department of Astronomy and Astrophysics, 50 St. George Street, University of Toronto, ON M5S 3H4, Canada
[17] Dunlap Institute for Astronomy and Astrophysics, 50 St. George Street, University of Toronto, ON M5S 3H4, Canada
[18] Anton Pannekoek Institute for Astronomy, University of Amsterdam, Science Park 904, 1098 XH Amsterdam, The Netherlands
[19] ASTRON, Netherlands Institute for Radio Astronomy,Oude Hoogeveensedijk 4, 7991 PD Dwingeloo, The Netherlands
[20] CSIRO Space & Astronomy, Parkes Observatory, P.O. Box 276, Parkes NSW 2870, Australia
[21] Dominion Radio Astrophysical Observatory, Herzberg Research Centre for Astronomy and Astrophysics, National Research Council Canada, P.O. Box 248, Penticton, BC V2A 6J9, Canada
[22] International Centre for Radio Astronomy Research (ICRAR), Curtin University, Bentley WA 6102, Australia
[23] Kavli Institute for the Physics and Mathematics of the Universe (Kavli IPMU), 5-1-5 Kashiwanoha, Kashiwa, 277-8583, Japan
[24] Division of Science, National Astronomical Observatory of Japan,2-21-1 Osawa, Mitaka, Tokyo 181-8588, Japan
[25] Department of Physics and Astronomy, York University, 4700 Keele Street, Toronto, ON MJ3 1P3, Canada
[26] Perimeter Institute of Theoretical Physics, 31 Caroline Street North, Waterloo, ON N2L 2Y5, Canada
Received 2024 October 30; revised 2024 December 10; accepted 2024 December 12; published 2025 January 21

Abstract

We report the discovery of the repeating fast radio burst (FRB) source FRB 20240209A using the Canadian Hydrogen Intensity Mapping Experiment (CHIME)/FRB telescope. We detected 22 bursts from this repeater between 2024 February and July, 6 of which were also recorded at the Outrigger station k'ni?atn k'l⌣stk'masqt (KKO). The multiple very long baseline interferometry localizations using the 66 km long CHIME–KKO baseline, each with a different baseline vector orientation due to the repeater's high decl. of ∼86°, enabled the combined localization region to be constrained to $1'' \times 2''$. We present deep Gemini optical observations that, combined with the FRB localization, enabled a robust association of FRB 20240209A to the outskirts of a luminous galaxy ($P(O|x) = 0.99$; $L \approx 5.3 \times 10^{10} L_{\odot}$). FRB 20240209A has a projected physical offset of 40 ± 5 kpc from the center of its host galaxy, making it the FRB with the largest host galaxy offset to date. When normalized by the host galaxy size, the offset of FRB 20240209A ($5.1\,R_{\rm eff}$) is comparable to that of FRB 20200120E ($5.7\,R_{\rm eff}$), the only FRB source known to originate in a globular cluster. We consider several explanations for the large offset, including a progenitor that was kicked from the host galaxy or in situ formation in a low-luminosity satellite galaxy of the putative host, but find the most plausible scenario to be a globular cluster origin. This, coupled with the quiescent, elliptical nature of the host as demonstrated in our companion Letter, provides strong evidence for a delayed formation channel for the progenitor of the FRB source.

[27] NHFP Einstein Fellow.
[28] Banting Fellow, McGill Space Institute (MSI) Fellow, and FRQNT Postdoctoral Fellow.

Unified Astronomy Thesaurus concepts: Radio bursts (1339); Radio transient sources (2008); Very long baseline interferometry (1769); Galaxies (573)

1. Introduction

Fast radio bursts (FRBs) are ∼ micro-to-millisecond-duration bursts of radio emission originating from extragalactic distances (E. Petroff et al. 2022). While thousands of FRBs have been detected, their origins remain unknown. Most FRB progenitor models involve stellar populations such as neutron stars and magnetars (W. Lu & P. Kumar 2018; B. D. Metzger et al. 2019; W. Lu et al. 2020; C. D. Bochenek et al. 2021). Some FRBs repeat, which rules out cataclysmic progenitor models for at least this class of FRBs. Repeating FRBs have varying burst activity rates, with some having sudden periods of heightened activity (A. E. Lanman et al. 2022; K. Nimmo et al. 2023; Y.-K. Zhang et al. 2023), while one repeater has bursts clustered in periodic activity windows (CHIME/FRB Collaboration et al. 2020a). The detection of repeat FRB-like bursts from a Galactic magnetar (C. D. Bochenek et al. 2020; CHIME/FRB Collaboration et al. 2020b) makes a strong case for magnetars as the origin of at least some FRBs.

Localizing FRBs to their local environments and host galaxies is one of the primary ways to uncover their origins. One-off FRBs have been localized to their host galaxies via connected-element interferometry (S. Bhandari et al. 2020; K. M. Rajwade et al. 2022; C. J. Law et al. 2024c), and follow-up of repeating FRBs has enabled their localization to their local environments via very long baseline interferometry (VLBI; B. Marcote et al. 2017, 2020; F. Kirsten et al. 2022; K. Nimmo et al. 2022b; T. Cassanelli et al. 2024; D. M. Hewitt et al. 2024a). There is some indication that FRBs preferentially occur in star-forming galaxies, with only a handful of FRBs localized to quiescent environments (K. Sharma et al. 2024). Additionally, nonrepeating FRBs are claimed to predominantly have spiral host galaxies (A. G. Mannings et al. 2021; M. Bhardwaj et al. 2024), with only one FRB having a candidate elliptical host (K. Sharma et al. 2024). Repeating FRBs have been localized to a variety of local environments, from extreme magneto-ionic environments within dwarf star-forming galaxies (S. Chatterjee et al. 2017; D. Michilli et al. 2018; C. H. Niu et al. 2022; R. Anna-Thomas et al. 2023) to a globular cluster (GC) of the massive spiral galaxy M81 (F. Kirsten et al. 2022). These varying local environments and host galaxies indicate that FRBs can occur in regions of both high and low star formation, and thus both prompt and delayed formation channels for FRB progenitors are possible.

The Canadian Hydrogen Intensity Mapping Experiment (CHIME)/FRB project (CHIME/FRB Collaboration et al. 2018) has detected the largest number of FRBs, both repeating and nonrepeating (E. Fonseca et al. 2020; CHIME/FRB Collaboration et al. 2021; CHIME/FRB Collaboration et al. 2023). Some of these FRBs have channelized raw voltage data (hereafter referred to as baseband data[29]) saved; however, interferometric localizations using the baseband data from CHIME alone can only provide an angular precision of $\sim 1'$ (D. Michilli et al. 2023), which is not precise enough to associate most FRBs to their host galaxies (T. Eftekhari & E. Berger 2017). Consequently, CHIME/FRB is building three Outrigger telescopes to form a VLBI array with CHIME to be able to localize FRBs with subarcsecond precision (C. Leung et al. 2021; J. Mena-Parra et al. 2022; T. Cassanelli et al. 2024; P. Sanghavi et al. 2023; S. Andrew et al. 2024; A. E. Lanman et al. 2024; C. Leung et al. 2024; A. B. Pearlman 2024).

Here we report, after ∼1500 hr of CHIME/FRB exposure over a period of 6 yr, the discovery of an active repeater FRB 20240209A. Using VLBI between CHIME and one of the outrigger stations k'ni?atn k'l_stk'masqt[30] (KKO; A. E. Lanman et al. 2024), we have localized FRB 20240209A to ∼ arcsecond precision. In Section 2, we describe the observations of this source and provide its burst rate estimates. In Section 3, we present the CHIME–KKO localization. The identification and nature of the host galaxy for this repeater are discussed in Section 4. In Section 5, we compare the properties of this FRB source to other repeating FRBs and make predictions about the possible progenitors based on the localization region and host galaxy. A detailed discussion about the host galaxy properties is presented by T. Eftekhari et al. (2025).

2. Observations

CHIME is a transit radio telescope located at the Dominion Radio Astrophysical Observatory near Penticton, British Columbia. It has a large field of view of $>200\,\mathrm{deg}^2$, a wide frequency bandwidth of 400–800 MHz, and records data in the east–west (E-W) and north–south (N-S) linear polarization bases (CHIME Collaboration et al. 2022). The CHIME/FRB project uses the CHIME instrument to continuously scan the entire Northern sky and search for FRBs in a multistage process described by CHIME/FRB Collaboration et al. (2018). CHIME/FRB records intensity (Stokes I) data with 0.98 ms time resolution for all candidate FRB events with signal-to-noise ratio (SNR) of SNR > 8. It also records baseband data with a 2.56 μs time resolution for events with SNR > 12 and for all events identified as candidate repeaters with SNR > 10.

The CHIME/FRB Outrigger station KKO provides a 66 km long E-W baseline with CHIME. The statistical localization precision achievable for this baseline for an event of SNR = 12 and having a bandwidth of 400 MHz is $\sim 1''$ (A. E. E. Rogers 1970). However, the realistic CHIME–KKO localization accuracy, which also includes systematic errors, is $\sim 2''$ along the baseline vector (A. E. Lanman et al. 2024). KKO has 1/16 the collecting area of CHIME and is very similar to CHIME in terms of its optical design, as well as its analog and digital systems. It is tilted by $\sim 0.^{\circ}5$ from the zenith in order to see the same sky as CHIME. KKO does not have an FRB detection backend, but it continuously buffers baseband data in a rolling buffer. CHIME/FRB sends FRB triggers to KKO for bursts with SNR > 15, upon which ∼100 ms of the buffered data around the time of the FRB are saved to disk at KKO such that the data in each frequency channel follows the dispersive sweep of the FRB. Note that in this Letter we use CHIME/FRB to refer to the central telescope system that searches for FRBs in real time, while we use KKO to refer to the Outrigger

[29] We note that while we have used the term "baseband data" to refer to channelized voltage data, historically, it has been used to refer to voltage data prior to channelization.

[30] From the upper Similkameen language, this translates to "a listening device for outer space."

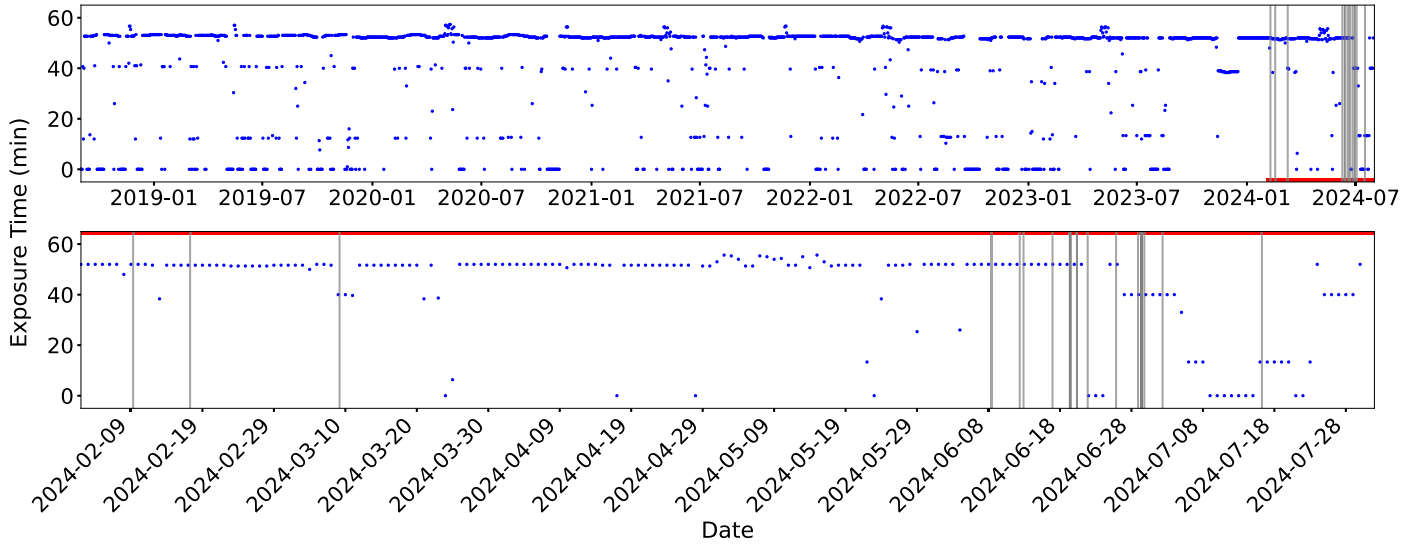

Figure 1. Total daily exposure time (UTC and topocentric at CHIME near Penticton, Canada) at the position of FRB 20240209A (blue points) and detection times of the repeat bursts (gray vertical lines). The top panel shows the exposure times since CHIME/FRB began operations. The red line indicates a window around the time the repeater became active, and the bottom panel is zoomed in on that window. The source had a median total exposure of approximately 55 minutes per day, which includes upper and lower transits having median exposures of 13 minutes and 39 minutes, respectively. Days with lower exposure are due to system shutdowns. The exposure is slightly higher on certain days every year due to an additional fractional sidereal transit of the source on the same solar day.

station that can trigger baseband data recording when a burst is detected by the central system.

FRB 20240209A was first detected on 2024 February 9 at 07:10:14 UTC (topocentric at CHIME near Penticton, Canada). Since then, 21 repeat bursts with real-time positions and dispersion measures (DMs) consistent with the first burst have been detected, until 2024 July 31. Fifteen of these bursts are reported by V. Shah & CHIME/FRB Collaboration (2024). Of the 22 bursts, 12 have only intensity data, while 10 have both intensity and baseband data. Six baseband bursts were also recorded at KKO. The timeline of the burst detections are shown in Figure 1 and the burst properties are listed in Table 2 in Appendix A, which also provides details about how the burst properties were estimated. Figure 2 shows the dynamic spectrum of the 10 bursts with baseband data, along with a frequency-channel-integrated time series, and a time-integrated spectrum. These burst profiles were obtained by beamforming the baseband data to the VLBI position of FRB 20240209A (see Table 1). It is evident that most bursts from this repeater are narrowband, having a fractional bandwidth of 20%–50% within the CHIME observing band. We note that following the burst activity in July, we did not detect any bursts from this repeater until another cluster of activity in 2024 October. However, we limit the analysis in this Letter to the bursts detected until 2024 July 31.

Following the announcement of the discovery of FRB 20240209A during its heightened activity in 2024 June (V. Shah & CHIME/FRB Collaboration 2024), the Northern Cross FRB collaboration reported the discovery of a single burst detected during a follow-up campaign (A. Geminardi et al. 2024). The burst was detected on 2024 July 2 at 21:24:24.540 UTC at 400 MHz. CHIME/FRB also detected a burst on the same day at 08:36:06 UTC at 400 MHz. C. J. Law et al. (2024) followed up the source with the Karl G. Jansky Very Large Array (VLA) in two 2 hr segments on 2024 July 2 and 2024 July 5 and did not detect any bursts at the observing frequency of 1–2 GHz; these observations did not overlap with CHIME detections. During the heightened activity of FRB 20240209A in 2024 October, O. S. Ould-Boukattine et al. (2024) detected a single burst at 1.3 GHz using the Westerbork RT-1 telescope after 350 hr of observations.

2.1. Burst Rate Estimate

The total exposure to the source was estimated using the functionality described in CHIME/FRB Collaboration et al. (2021). Various metrics throughout different data processing stages were recorded to characterize the total uptime and variation in sensitivity of the entire CHIME/FRB system. This information was combined with the beam model[31] in order to account for times when a source transits through the FWHM of our formed beams at 600 MHz.

The exposure was queried using the best-known position of FRB 20240209A (V. Shah & CHIME/FRB Collaboration 2024). Due to the high decl. of this source, it is circumpolar in CHIME's field of view, i.e., it has two transits separated into upper and lower transits (CHIME/FRB Collaboration et al. 2021). It is important to note that the two transits have different sensitivities for the same source. CHIME's exposure to this source from 2018 August 28 to 2024 July 31 was ∼362 hr in the upper transit and ∼1123 hr in the lower transit, amounting to a total of ∼1485 hr.

CHIME/FRB detected 13 repeat bursts in the upper transit and 9 repeat bursts in the lower transit. Out of these, only two bursts, one each in the upper and lower transits, were detected within the FWHM of our formed beams at 600 MHz. Since our exposure calculation only accounts for the source transit time through the FWHM of our beams, only these two bursts can be used for burst rate calculation, given our adopted definition of exposure. Using the daily exposure time toward the source, we obtain a burst rate of $5\,\mathrm{hr}^{-1}$ above a fluence threshold of 1.5 Jy ms and $2\,\mathrm{hr}^{-1}$ above a fluence threshold of 0.9 Jy ms in the upper and lower transits, respectively. The fluence thresholds were estimated using the methodology described by A. Josephy et al. (2019), CHIME/FRB Collaboration et al. (2021), and CHIME/FRB Collaboration (2025, in preparation).

[31] https://chime-frb-open-data.github.io/beam-model/

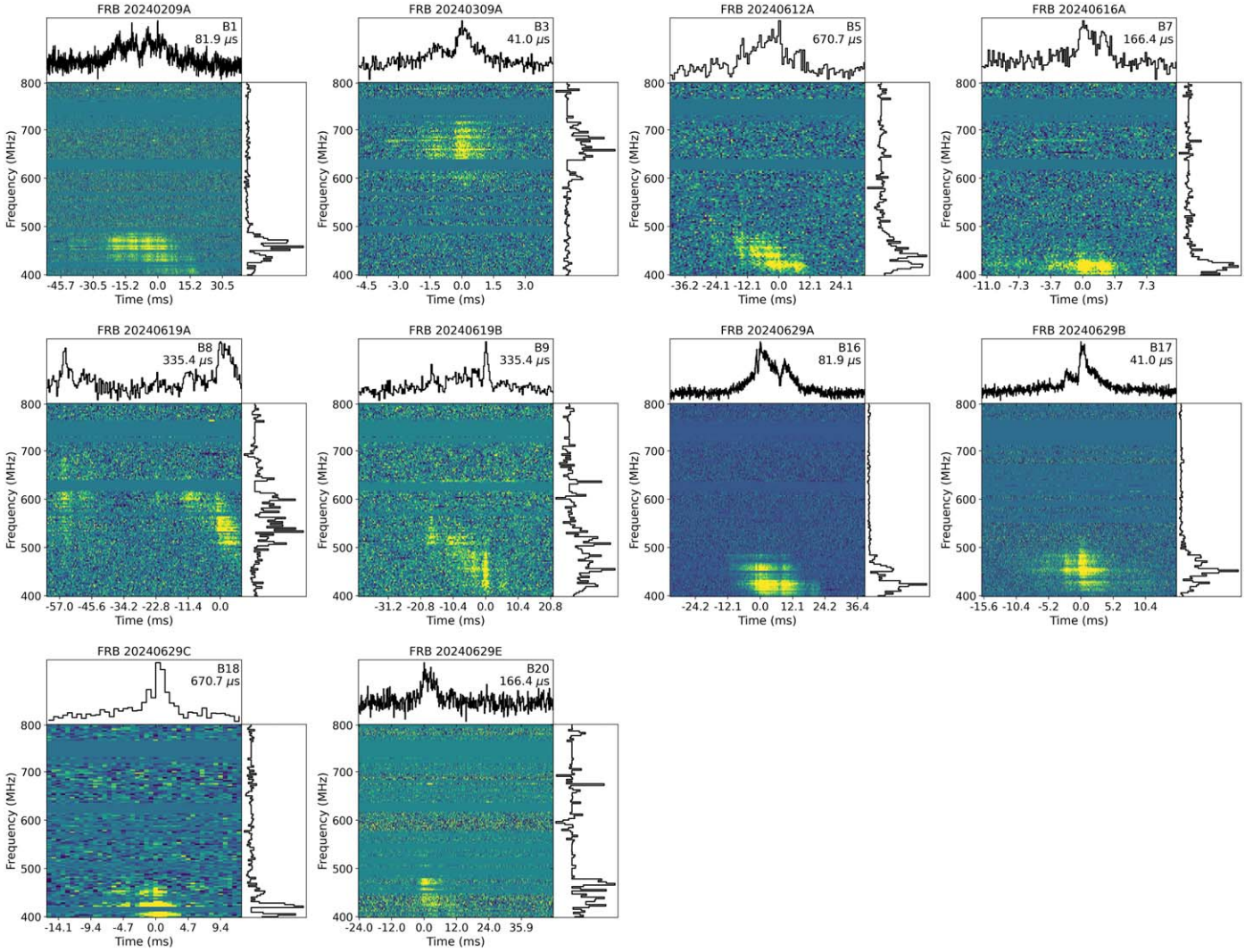

Figure 2. Dynamic spectra, frequency-integrated profiles, and time-integrated spectra of the 10 repeat bursts from FRB 20240209A that have baseband data saved at CHIME. The time resolution at which each burst is plotted along with the burst number (see Table 2) is indicated in the top-right corner, and the Transient Name Server (TNS) name of the burst is provided in the heading of each plot.

Table 1
Parameters for the 1σ CHIME–KKO VLBI Localization Ellipse for FRB 20240209A, with the Center of the Ellipse Defined in the ICRS J2000 Reference Frame

R.A.	Decl.	Semiminor axis	Semimajor axis	Position Angle
$19^{h}19^{m}33^{s}$	$+86°03'52''$	$1''.08$	$2''.12$	$9°.54$

Given that CHIME/FRB sees the source for the same amount of time each day, both within and outside the FWHM of our formed beams, it is apparent from Figure 1 that the burst activity of FRB 20240209A varied significantly over the course of its activity period. The initial activity of the source was characterized by sparse burst detections, with consecutive bursts separated by multiple days, followed by a period of no burst detections for ~3 months. The source suddenly became very active in 2024 June, with 17 out of the 22 bursts detected over the course of a month. The peak burst activity was reached on 2024 June 29 when CHIME/FRB detected five bursts from this source. This increase in the detection rate signifies that the source entered a high-activity period fairly recently, and more broadly that some FRBs may rapidly transition from years of quiescence to hyperactivity on timescales of weeks to months. Such burst activity, from quiescence to hyperactivity, has also been seen for sources such as FRB 20121102A (D. Li et al. 2021), FRB 20201124A (A. E. Lanman et al. 2022), and FRB 20220912A (R. McKinven & CHIME/FRB Collaboration 2022). Additionally, as shown in Figure 1, CHIME had limited exposure in the direction of this repeater following its peak burst activity because the FRB search engine gets shut down when the temperature in the computing container becomes too high during the summer months. Thus, there is a possibility that additional bursts from this source were missed during its transit in July.

3. Localization

Baseband data for six FRB 20240209A bursts were saved at the KKO site, allowing six separate CHIME–KKO VLBI[32]

[32] The 66 km long CHIME–KKO baseline is not a "very long" baseline *per se*. However, VLBI can often mean a nonconnected interferometer with different clock signals at different stations where the voltage data need to be digitally shipped and correlated retrospectively. We use the term "VLBI" in that context in this Letter.

localizations for this repeater. For each of these bursts, full-array baseband data were beamformed toward the best-fit FRB position found from the baseband localization pipeline, R.A. (J2000) = $19^{h}19^{m}39\overset{s}{.}84$, decl. (J2000) = $+86°03'44.28''$ (D. Michilli et al. 2023; V. Shah & CHIME/FRB Collaboration 2024), as well as the position of the source J0117+8928 from the Very Long Baseline Array Radio Fundamental Catalog,[33] which was used as the phase calibrator. This beamforming was done for both the CHIME and KKO stations. J0117+8928 was the best choice of calibrator, as it is unresolved on the CHIME–KKO baseline, and detected with a cross-correlation SNR > 50. It also has a small angular separation of $\sim 4°$ from the FRB position and is always within the primary beam of the CHIME and KKO cylinders because of its very high decl. of $89\overset{\circ}{.}47$. For each of the six target bursts, CHIME and KKO data were coherently de-dispersed using a DM of 176.518 pc cm^{-3}, cross-correlated using the `PyFX` VLBI correlator (C. Leung et al. 2024), and then phase-referenced to the cross-correlated visibilities of J0117+8928. The target visibilities were integrated for the duration of the burst while the calibrator visibilities were integrated for the entire $\sim$100 ms duration of the baseband dumps. The calibrated visibilities were obtained for both the E-W and N-S polarizations. Since the phase calibrator data were recorded simultaneously with the burst data, no clock calibration was necessary (C. Leung et al. 2021). Though CHIME and KKO view the source through different sightlines through the ionosphere, this is not a dominant source of error for the short CHIME–KKO baseline at the observing frequencies we use at 400–800 MHz (A. E. Lanman et al. 2024). Moreover, the small angular separation between the target and the calibrator ensured that any differential ionospheric delays were well within our localization uncertainty. Only the visibility data for frequency channels that had signal were used for localization, which amounted to 60–100 MHz of bandwidth used for the narrowband bursts from this repeater.

A grid of R.A. and decl. centered on the baseband localization was searched to determine the CHIME–KKO VLBI localization position using a "delay mapping" technique (see Equations (12), (13), and (19) of A. E. Lanman et al. 2024). The differential geometric delay between CHIME and KKO with respect to the initial pointing was estimated for each point in the grid and compared to the differential geometric delay obtained from the calibrated visibilities, which gave a localization likelihood (see Equation (A1) of C. Leung et al. 2024). The uncertainty on the localization was determined by the uncertainty on the delay, which is typically $\sim$1 ns for the CHIME–KKO baseline (A. E. Lanman et al. 2024). However, since the bursts from this repeater are narrowband, a more conservative delay uncertainty of 2 ns (assumed to be Gaussian distributed) was used to account for unknown systematic errors and residual ionospheric delays (see Figure 13 of A. E. Lanman et al. 2024). If the delays obtained from the E-W and N-S calibrated visibilities differed by more than 1 ns, the polarization with the higher cross-correlation SNR was used for localization. Localization likelihoods for one or more polarizations for each of the six bursts were multiplied to obtain the combined localization. This localization region was inflated by convolving it with a two-dimensional (2D) Gaussian having $\sigma = 1''$ to account for correlated systematic errors (see Appendix B for more details), giving a final localization ellipse of dimensions $\sim 1'' \times 2''$.

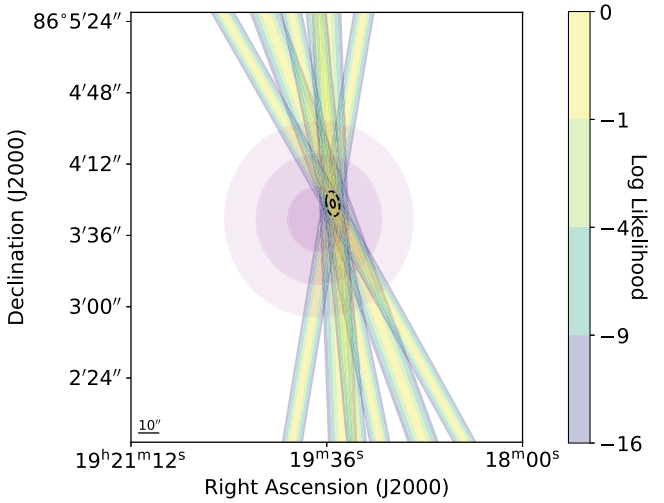

Figure 3. The purple shaded ellipses show the 1σ, 2σ, and 3σ CHIME-only baseband localization region for FRB 20240209A. The contour stripes show the CHIME–KKO VLBI localization regions for six repeat bursts, each constrained along the baseline vector. The black ellipses show the 1σ and 3σ combined VLBI localization region after accounting for correlated systematic errors.

In Figure 3, the purple ellipses show the 1σ, 2σ, and 3σ CHIME-only baseband localization regions for FRB 20240209A (V. Shah & CHIME/FRB Collaboration 2024). The contour stripes show the six CHIME–KKO localizations, with the solid and dashed black ellipses delimiting the 1σ and 3σ combined localization regions, respectively. The multiple CHIME–KKO localizations, each with a different baseline vector orientation due to the repeater's high decl., permitted the combined VLBI localization region to be constrained along several axes. The parameters for the CHIME–KKO 1σ localization ellipse are listed in Table 1.

4. Host Galaxy

4.1. Deep Imaging and Host Galaxy Association

We imaged the field of FRB 20240209A with the Gemini Multi-Object Spectrograph (GMOS) mounted on the 8 m Gemini-North telescope on UT 2024 August 8 (PI: T. Eftekhari), for a total exposure of 1 hr in the r band. We used the `POTPyRI pipeline`[34] to apply bias and flat-field corrections and coadd the images. We performed astrometric calibration using sources in common with the Gaia Data Release 3 catalog with an astrometric tie rms of $0\overset{''}{.}06$. We performed aperture photometry of the host galaxy within a $14''$ radius aperture and calculated a magnitude $r = 16.79 \pm 0.02$ mag (AB).

To determine the most probable host galaxy, we utilized the Probabilistic Association of Transients to their Hosts method (PATH; K. Aggarwal et al. 2021), a Bayesian framework for associating transients with their hosts. We adopted the default "inverse" prior that accounts for the higher incidence of faint galaxies on the sky (i.e., a Jeffreys prior for apparent magnitude) and an underlying exponential distribution scaled by one-half the half-light radius as the prior for the offset distribution (R. M. Shannon et al. 2024). For the prior probability that the host is unseen, we assumed a conservative

[33] https://astrogeo.org/sol/rfc/rfc_2024a/

[34] https://github.com/CIERA-Transients/POTPyRI

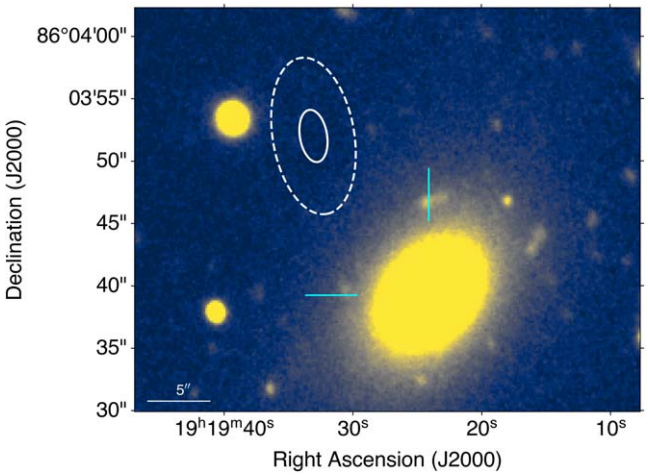

Figure 4. Gemini r-band image showing the host galaxy of FRB 20240209A (cyan crosshairs) and the 1σ (white solid) and 3σ (white dashed) localization ellipses. The source to the east of the localization ellipse is a star. The 3σ limiting magnitude is $r \gtrsim 25.9$ mag (corrected for Galactic extinction).

value of $P(U) = 0.15$ given the 3σ limiting magnitude of the Gemini/GMOS image of $r \approx 25.9$ mag (AB, corrected for a Galactic extinction of $A_r = 0.266$ mag). To identify galaxy candidates, we utilized `Source Extractor` on a $40'' \times 40''$ region centered on the FRB position. We performed aperture photometry on each of the identified sources and fed as input to PATH the extinction-corrected magnitudes, source positions, and estimates for the angular sizes. The host of FRB 20240209A was robustly identified with a posterior probability $P(O|x) = 0.99$ (Figure 4).

Using the spectrum of the host galaxy, we classify it as a quiescent galaxy at $z = 0.1384 \pm 0.0004$ (T. Eftekhari et al. 2025), adding to the small sample of FRB hosts in quiescent environments (K. W. Bannister et al. 2019; K. Sharma et al. 2023; C. J. Law et al. 2024; K. Sharma et al. 2024). The properties of FRB 20240209A are especially notable given no FRB associated with a quiescent galaxy has yet been observed to repeat. FRB 20240209A is also the first FRB localized to a galaxy with unambiguous elliptical morphology (T. Eftekhari et al. 2025), with only one other nonrepeating FRB having a candidate elliptical host (K. Sharma et al. 2024). The global host galaxy properties, especially its extremely old stellar population (∼11 Gyr; T. Eftekhari et al. 2025), coupled with the large host galaxy offset evident in Figure 4, support a delayed formation channel for the progenitor of FRB 20240209A. We discuss these implications in Section 5.

In order to verify the consistency of the host galaxy redshift with the observed DM of FRB 20240209A, we use the joint probability distribution of redshift and extragalactic DM for CHIME repeaters, developed by C. W. James (2023), to estimate a probabilistic maximum redshift. We use the NE2001 estimate of 55.5 pc cm^{-3} for the Milky Way (MW) disk DM contribution (J. M. Cordes & T. J. W. Lazio 2002; S. K. Ocker & J. M. Cordes 2024), which is consistent with the YMW16 estimate of 52.2 pc cm^{-3} (J. M. Yao et al. 2017). We assume both the MW halo DM contribution ($\mathrm{DM_{MW,halo}}$) and host galaxy DM contribution $\mathrm{DM_{host}}$ are 0 pc cm^{-3} in order to obtain a more conservative $z_{\max}$. Given that the extragalactic DM is the total DM minus the NE2001 contribution, the resulting 95% upper limit on redshift is $z_{\max} = 0.19$. Thus, the redshift of the putative host galaxy is consistent with the probabilistic maximum redshift given by the DM of FRB 20240209A but suggests a small contribution to the DM from the local environment and host galaxy of the FRB.

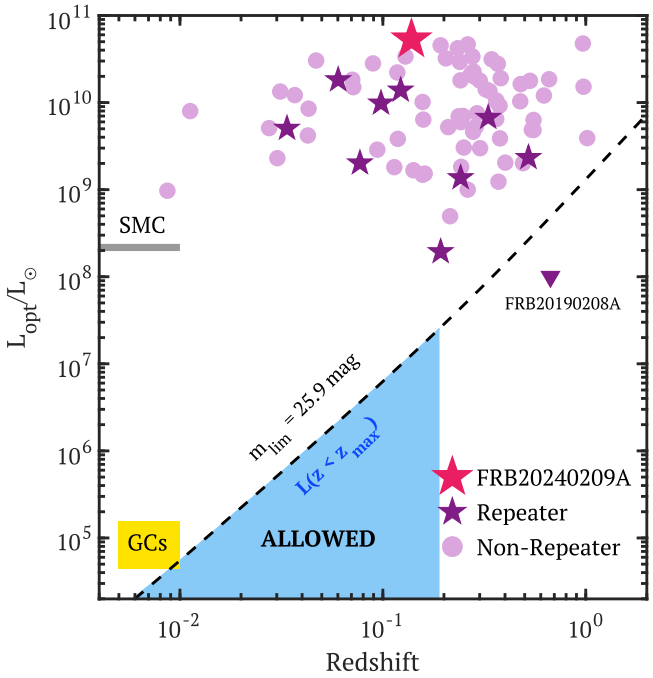

Figure 5. Optical luminosity vs. redshift for the host galaxy of FRB 20240209A (red star) and other FRB hosts in the literature (V. Ravi et al. 2019; A. C. Gordon et al. 2023; K. Lee-Waddell et al. 2023; M. Bhardwaj et al. 2024; L. Connor et al. 2024; A. L. Ibik et al. 2024a; C. J. Law et al. 2024; R. M. Shannon et al. 2024; K. Sharma et al. 2024); stars denote known repeaters while circles denote apparent nonrepeaters. The dashed line corresponds to the Gemini luminosity limit of $r \approx 25.9$ mag (3σ), for which parameter space above the line is ruled out for a source coincident with the KKO localization. The range of luminosity limits on a coincident source, set by the upper limit on the redshift inferred from the DM ($z_{\max} = 0.19$), is highlighted in the blue shaded region, corresponding to $\lesssim 2.5 \times 10^7\, L_{\odot}$. This is well below the luminosity of the Small Magellanic Cloud (gray horizontal line) and below the limit of the inferred luminosity for the host of FRB 20190208A (D. M. Hewitt et al. 2024b; purple triangle). The lower bound reaches the luminosities of GCs in elliptical galaxies (yellow box; e.g., J. Strader et al. 2006). The luminosity of the GC hosting the repeating FRB 20200120E ($L \approx 1.3 \times 10^5\, L_{\odot}$) falls toward the upper side of the yellow box (F. Kirsten et al. 2022; M. Bhardwaj et al. 2021).

To place the host of FRB 20240209A into context with the FRB host population, in Figure 5 we show the optical r-band luminosities[35] of FRB host galaxies as a function of the redshift; all magnitudes are corrected for Galactic extinction (V. Ravi et al. 2019; A. C. Gordon et al. 2023; K. Lee-Waddell et al. 2023; M. Bhardwaj et al. 2024; L. Connor et al. 2024; A. L. Ibik et al. 2024a; C. J. Law et al. 2024; R. M. Shannon et al. 2024; K. Sharma et al. 2024). We also include the inferred limit on the luminosity for the low-luminosity host of FRB 20190208A (D. M. Hewitt et al. 2024b). With $L \approx 5.3 \times 10^{10}\, L_{\odot}$, the putative host galaxy of FRB 20240209A is the most luminous FRB host galaxy to date, 3 times more than the most luminous host of a known repeating FRB (although only ≈10% more luminous than that of a nonrepeating FRB). Here we entertain the possibility that there exists an undetected source within the combined KKO localization. Our deepest Gemini imaging reaches a 3σ limit of $r \approx 25.9$ mag derived using the image FWHM of $0\farcs6$, which we translate to the

[35] In a few cases where the r band is not available, we use the i band.

required combination of luminosity and redshift to exist below our detection threshold (Figure 5). Given the redshift constraints from DM and the location of the FRB, one possibility is that of a satellite of the putative host at the same redshift ($z = 0.1384$), for which the Gemini limit requires that $L \lesssim 1.2 \times 10^7 L_\odot$. Alternatively, there may exist a galaxy at a redshift different from that of the putative host. For $z < z_{\rm max}$ where $z_{\rm max} = 0.19$ (95% confidence) the Gemini limit requires $L \lesssim 2.5 \times 10^7 L_\odot$. Even for the most optimistic case of $z = z_{\rm max}$, our limits imply a luminosity $\gtrsim$10 times less than that of any other known FRB host galaxy with a redshift (A. C. Gordon et al. 2023; S. Bhandari et al. 2023). We note that the dwarf host of FRB 20190208A does not have a redshift, but has a range of luminosities of $\approx 10^7$–$10^8 L_\odot$ inferred from the DM (D. M. Hewitt et al. 2024b), potentially comparable to the limit for FRB 20240209A. Thus, if FRB 20240209A originated from an undetected galaxy, it would need to be extreme in terms of its low luminosity compared to the rest of the FRB population. We discuss this in the context of possible progenitors in Section 5.

5. Discussion

The burst properties, activities, and counterparts of FRBs give clues about their emission mechanisms, progenitor types, and local environments. We compare these attributes of FRB 20240209A to those of other repeating FRBs. Moreover, the host galaxy properties and location of the FRBs within their hosts help identify the most viable FRB formation channels possible for specific environments. We therefore discuss the implications for the progenitor of FRB 20240209A based on its offset from the putative host.

5.1. Comparison with Other Repeaters

5.1.1. Burst Properties

The wide temporal widths and narrowband nature of FRB 20240209A bursts are consistent with what is observed in the broader repeater population (Z. Pleunis et al. 2021a). Moreover, bursts B1, B5, B8, B9, and B16 clearly show a downward-drifting morphology in the frequency–time space. Among repeaters, FRB 20121102A is known to emit isolated bursts of microsecond duration (M. P. Snelders et al. 2023), while FRB 20200120E shows substructure down to a timescale of ∼60 ns in submillisecond-duration bursts (W. A. Majid et al. 2021; K. Nimmo et al. 2022a). If FRB 20240209A emitted such narrow bursts, they would have to be brighter than the wider bursts in order to be detected by the CHIME/FRB backend, which detects with a time resolution of ∼1 ms. Moreover, the bursts from FRB 20200120E are 2–3 orders of magnitude less energetic than those from other repeating FRBs, and thus easily detectable for FRB 20200120E only due to the proximity of this source located 3.6 Mpc away. Although FRB 20240209A does not show such isolated narrow bursts, it does show evidence of structures of varying timescales within the broader burst envelope, especially in burst B1. Such structures are also seen in bursts from other repeaters (K. Nimmo et al. 2021; D. M. Hewitt et al. 2023). Thus, the morphological features of FRB 20240209A are consistent with those of other repeaters and suggest that FRB 20240209A potentially has the same emission mechanism and progenitor type as other repeating FRBs. However, this does not preclude the progenitor of FRB 20240209A from having a different formation channel compared to other repeaters.

The brightest burst from FRB 20240209A in our sample is the first burst detected from this source, which has a structure-maximizing DM of 176.49 pc cm^{-3}. The DMs of the repeat bursts listed in Table 2 are largely consistent. We do not consider any apparent DM variation to be intrinsic to the source as it is nontrivial to disentangle DM variation from downward-drifting morphology, especially at the coarser time resolution for some bursts. Moreover, the DM variation of >1 pc cm^{-3} for FRB 20121102A occurs over a period of years (D. Li et al. 2021). Thus, significant DM variation is not expected in the FRB 20240209A bursts listed here, which span a period of a few months.

5.1.2. Burst Activity

The daily exposure of CHIME toward the position of FRB 20240209A allows us to monitor the activity of the source. FRB 20240209A was first detected in 2024 February and we estimate a burst rate of 5 hr^{-1} above a fluence threshold of 1.5 Jy ms and 2 hr^{-1} above a fluence threshold of 0.9 Jy ms in the upper and lower transits, respectively. Following its initial detections, the source had a sudden period of heightened burst activity in 2024 June. A sudden increase in burst activity has also been seen in other repeaters: the first example is from the CHIME/FRB observation of a period of high burst activity from the repeater FRB 20201124A, with the peak burst rate reaching up to 92 day^{-1} and 201 day^{-1} with a 90% fluence threshold of 19 Jy ms during this period in the CHIME band (A. E. Lanman et al. 2022). For this source, FAST saw a peak burst rate of 542 hr^{-1} (Y.-K. Zhang et al. 2022) in their 1–1.5 GHz observing band with a 90% fluence threshold of ∼0.03 Jy ms. For FRB 20200120E, K. Nimmo et al. (2023) observed a period of burst activity with the Effelsberg telescope at 1.4 GHz, where the source emitted 53 bursts within 43 minutes above a fluence of 0.04 Jy ms. Y.-K. Zhang et al. (2023) observed FRB 20220912A with the FAST telescope and observed an event rate up to 390 hr^{-1} with a 90% fluence threshold of ∼0.014 Jy ms. Most recently, FAST also observed FRB 20240114A to have a burst rate up to ∼500 hr^{-1} above a fluence of 0.015 Jy ms, an increase in burst activity by over an order of magnitude compared to observations conducted just over a week prior (J. Zhang et al. 2024). The sudden increase in activity of FRB 20240209A is thus consistent with other repeaters, although a direct comparison of burst rates across different frequency bands and fluence thresholds requires a more detailed analysis.

As discussed in Section 2, apart from the CHIME-detected bursts, there are only two other reported detections of FRB 20240209A. The Northern Cross FRB collaboration detected a single burst at 400 MHz in 20 hr of observation (A. Geminardi et al. 2024), while the Westerbork RT-1 telescope detected a single burst at 1.3 GHz in 350 hr of observation (O. S. Ould-Boukattine et al. 2024). This is seemingly in contrast to other repeaters that have been highly active across a wide frequency band—all the aforementioned FRB repeaters, which had follow-up burst activity monitoring campaigns at >1 GHz, were discovered by CHIME/FRB at 400–800 MHz. Other repeating FRBs with detections across various frequency bands include FRB 20121102A (from ∼600 MHz to ∼8 GHz, though seemingly preferentially at higher frequencies; V. Gajjar et al. 2018; A. Josephy et al. 2019) and FRB 20180916B (from

∼110 MHz to ∼8 GHz Z. Pleunis et al. 2021b; S. Bethapudi et al. 2023). A deeper analysis is required to study the burst activity of FRB 20240209A across different frequency bands.

5.1.3. Limits on a Persistent Radio Counterpart

Only FRB 20121102A and FRB 20190520B are confidently associated with compact persistent radio sources (PRSs) that are coincident with their positions (S. Chatterjee et al. 2017; C. H. Niu et al. 2022). Interestingly, these are also the only two FRBs known to have Faraday rotation measures (RMs) as high as $\approx 10^4$–10^5 rad m^{-2} (D. Michilli et al. 2018; R. Anna-Thomas et al. 2023). FRB 20201124A has a coincident radio source, which is interpreted as a candidate PRS (G. Bruni et al. 2024) or star formation (Y. Dong et al. 2024). We performed an archival search for compact persistent radio emission at the position of FRB 20240209A, utilizing CIRADA[36] cutouts to extract a 1 arcmin^2 region surrounding the VLBI position. The VLA Sky-Survey Quicklook (VLASS-QL; M. Lacy et al. 2020) was the only radio survey with available observations of the field of FRB 20240209A. We found no evidence of any PRS emission within the 3σ localization regions above the 5σ rms threshold of 600 μJy. Assuming $z = 0.1384$, we place a 5σ upper limit on the spectral luminosity of any PRS counterpart of $L_{3.0\mathrm{GHz}} \lesssim 3 \times 10^{29}$ erg s^{-1} Hz^{-1}. In comparison to those available in the literature, a PRS akin to those associated with FRB 20121102A and FRB 20190520B, which fall within the spectral luminosity ranges of $L_{1.7\mathrm{GHz}} \approx 1$–$3 \times 10^{29}$ erg s^{-1} Hz^{-1} (B. Marcote et al. 2017; S. Bhandari et al. 2023), would be on the cusp of the 5σ detection threshold provided by VLASS-QL. On the contrary, a lower-luminosity PRS akin to the candidate PRS associated with FRB 20201124A with $L_\nu \sim 5 \times 10^{27}$ erg s^{-1} Hz^{-1} (G. Bruni et al. 2024) would fall below the detection threshold.

C. J. Law et al. (2024) searched for a PRS at the FRB 20240209A position using VLA and found an unresolved radio source that is at or near the nucleus of the putative host. Given the large offset of FRB 20240209A from the putative host, this radio source is not associated with the FRB and instead may indicate the presence of a radio-loud active galactic nucleus in the host as discussed in T. Eftekhari et al. (2025). While a lower-luminosity PRS counterpart cannot be ruled out at this stage, FRB 20240209A currently joins the group of well-localized repeating FRBs with no observed compact radio counterparts (A. L. Ibik et al. 2024b).

5.2. Galactocentric Offset and Implications for the Progenitor of FRB 20240209A

One of the most notable features of FRB 20240209A is the offset from its host galaxy, which has implications for its progenitor. Thus, we use the combined CHIME–KKO localization to calculate the distribution of possible angular offsets between FRB 20240209A and its host galaxy center, weighted by the localization probability map. Using $z = 0.1384$ and Planck cosmology (Planck Collaboration et al. 2020), we calculate a projected physical offset of 40 ± 5 kpc (68% confidence). Since the host of FRB 20240209A is particularly large in extent (T. Eftekhari et al. 2025), it is informative to normalize the offset by the host galaxy size. We use the host effective radius $R_{\mathrm{eff}} = 7.78 \pm 0.03$ kpc from morphological fitting (T. Eftekhari et al. 2025) to calculate a host-normalized offset of $5.1 \pm 0.6\ R_{\mathrm{eff}}$, demonstrating a location well outside the locus of the host galaxy light. This large offset of FRB 20240209A from a luminous and quiescent host galaxy makes it stand apart from the majority of the FRB population, characterized primarily by star-forming galaxies at physical offsets of $\lesssim$10 kpc and host-normalized offsets of $\lesssim 2\ R_{\mathrm{eff}}$ (K. E. Heintz et al. 2020; A. G. Mannings et al. 2021; S. Bhandari et al. 2022; A. C. Gordon et al. 2023; K. Sharma et al. 2024).

For context, in Figure 6, we show the cumulative distribution of projected FRB host galaxy offsets for 6 repeating and 37 nonrepeating FRBs with available offset information in both physical and host-normalized units (A. G. Mannings et al. 2021; S. Bhandari et al. 2022; K. Sharma et al. 2024; M. N. Woodland et al. 2024). In physical units, the offset of FRB 20240209A exceeds the median FRB population offset of ≈5.4 kpc by a factor of 7; indeed, it has the largest host galaxy offset observed to date. While in host-normalized units, the offset of FRB 20240209A is 4 times larger than the median offset of $\approx 1.4\ R_{\mathrm{eff}}$, rivaled only by the offset of FRB 20200120E. Many FRB progenitor models invoke a magnetically powered neutron star (NS), called a magnetar, as the central engine (E. Platts et al. 2019). FRBs localized within star-forming regions can be produced by young magnetars formed via core-collapse supernovae. Thus, while the majority of the FRB population is consistent with magnetars created from core-collapse supernovae, the properties of FRB 20240209A challenge this interpretation, as the fraction of stars at $\sim 5\ R_{\mathrm{eff}}$ is extremely low. In the following subsections, we briefly consider three progenitor scenarios to explain the large offset from the putative host: a progenitor that (1) formed in situ in a GC associated with the massive host galaxy, (2) formed in situ in an undetected satellite dwarf galaxy of the massive galaxy, or (3) was kicked from its birthplace.

5.2.1. Globular Cluster Origin

For in situ progenitors, the localization of FRB 20200120E to a GC (F. Kirsten et al. 2022) demonstrated that at least some FRBs can originate in environments with older stellar progenitors. The extreme offset of FRB 20240209A could naturally be explained by the formation in a GC. To place this possibility into context, in Figure 6, we plot the cumulative distributions of projected physical offsets of GCs in the Milky Way (W. E. Harris 1996), M81 (J. B. Nantais & J. P. Huchra 2010; J. B. Nantais et al. 2010), and the elliptical galaxies NGC 821 (L. R. Spitler et al. 2008) and NGC 4278 (C. Usher et al. 2013). Since the galactocentric offsets of GCs can depend on the sizes of their host galaxies, it is equally informative to compare the host-normalized offsets. Thus, we also show the projected offset distributions in host-normalized units, using R_{eff} of 5.75 kpc (J. Lian et al. 2024), 3.5 kpc (K. Sheth et al. 2010), 5.1 kpc (S. Pellegrini et al. 2007) and 2.4 kpc (C. Usher et al. 2013) for the Milky Way, M81, NGC 821, and NGC 4278, respectively. We also show the projected offset of FRB 20200120E, which was precisely localized to a GC of the spiral galaxy M81 (M. Bhardwaj et al. 2021; F. Kirsten et al. 2022). We find that in terms of physical offsets, FRB 20240209A is consistent with the upper ≈10%–25% of the spatial distribution of GCs in ellipticals. When normalized by the host galaxy size, the offset of FRB 20240209A is still consistent with those of GCs in

[36] https://cirada.ca/

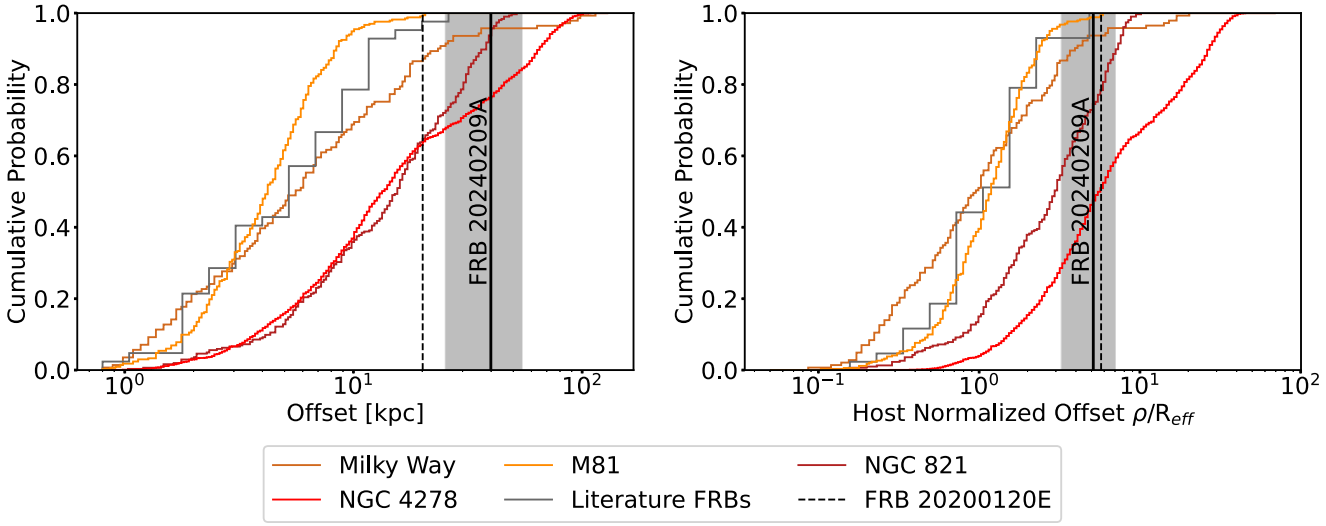

Figure 6. Projected physical offsets (left panel) and host-normalized offsets (right panel) of 43 FRBs that have robust host associations and offset information. Also shown are the projected physical and host-normalized offsets of GCs of the spiral galaxies Milky Way and M81, and of the elliptical galaxies NGC 821 and NGC 4278. The black dashed line shows the ∼20 kpc projected offset of FRB 20200120E, which is localized to a GC of M81. The black solid line shows the ∼40 kpc projected offset of FRB 20240209A with the gray shaded region showing the 3σ uncertainty on the offset based on the localization region. Based on its offset, FRB 20240209A is consistent with originating from a GC of its massive elliptical host galaxy.

elliptical galaxies in the upper ≈30%–50% of those distributions. Notably, the host-normalized offset of FRB 20200120E is very similar to the median value for FRB 20240209A (5.7 versus 5.1 $R_{\rm eff}$). Thus, this comparison clearly illustrates that based on offsets alone, it is plausible that FRB 20240209A could have originated from a GC.

In such a case, promising progenitor models for GC FRBs include magnetars formed via the accretion-induced collapse of a white dwarf (WD), or merger-induced collapse of a WD–WD, NS–WD, and NS–NS binary, in which dynamical interactions within the GC can increase the rates of such events (e.g., K. Kremer et al. 2021). Low-mass X-ray binaries (LMXBs) and ultraluminous X-ray sources (ULXs) are also viable given their occurrence in GCs (G. W. Clark 1975; T. J. Maccarone et al. 2007; K. C. Dage et al. 2021; N. Sridhar et al. 2021). Notably, based on deep X-ray measurements, A. B. Pearlman et al. (2024) ruled out ULXs and ∼30% of the brightest Milky Way–like LMXBs for FRB 20200120E. Thus, the association of FRB 20240209A to a ULX would make it distinct from FRB 20200120E.

5.2.2. Undetected Satellite Dwarf Galaxy

Another possibility is that the FRB originated in an undetected satellite dwarf galaxy. In such a case, there is no constraint on the age of the progenitor and prompt formation channels such as a magnetar formed via core-collapse supernova of a massive star are possible. However, as discussed in Section 4, such a galaxy would have $L \lesssim 1.2 \times 10^7\, L_\odot$ making it $\gtrsim$10 times less luminous than any other FRB host galaxy with known redshift. Moreover, this upper limit on luminosity falls toward the lower end of the luminosity range possible for the dwarf host of FRB 20190208A (D. M. Hewitt et al. 2024b), indicating further that the presence of an undetected satellite dwarf would be an extreme scenario in terms of host luminosity.

In Section 4, we derived a conservative 95% upper limit on the redshift of the FRB of $z_{\rm max} = 0.19$ assuming $0\,{\rm pc\,cm^{-3}}$ for $\rm DM_{MW,halo}$ and $\rm DM_{host}$. If we instead use $\rm DM_{MW,halo} = 30\,pc\,cm^{-3}$ and $\rm DM_{host} = 10\,pc\,cm^{-3}$, which are still on the lower end of the expected contributions (J. X. Prochaska & Y. Zheng 2019; S. Yamasaki & T. Totani 2020; A. M. Cook et al. 2023; K. Shin et al. 2023), we find $z_{\rm max} = 0.14$. This suggests that at the redshift of the FRB host galaxy of $z = 0.1384$, there is barely any DM contribution from the local environment and host galaxy of the FRB. This is in stark contrast to the hundreds of units of $\rm DM_{host}$ for the three FRBs known to reside in dwarf galaxies (S. P. Tendulkar et al. 2017; C. H. Niu et al. 2022; S. Bhandari et al. 2023). The two repeating FRBs out of these three FRBs in dwarf galaxies also exhibit very high RM values (D. Michilli et al. 2018; R. Anna-Thomas et al. 2023). Polarization analysis of FRB 20240209A will be done in future work and will give more clues about its local environment. Thus, based on DM budgeting, we infer that FRB 20240209A resides in a clean environment indicating that a GC origin is a more favorable scenario than a satellite dwarf galaxy origin. If correct, a low value of RM would be expected. Space-based imaging coupled with a more precise localization of FRB 20240209A is required to distinguish between the two possibilities.

5.2.3. Kicked Progenitor

It is possible that the progenitor of FRB 20240209A was kicked out of its host galaxy. Plausible progenitors include binary neutron star mergers (NS–NS) or WD–NS mergers, which in a small fraction of cases may produce indefinitely stable neutron stars (B. Margalit & B. D. Metzger 2019). Indeed, the high systemic velocities coupled with the long delay times relative to star formation can result in galactocentric offsets of tens of kpc (K. Belczynski et al. 2006). However, we find that only ≈15% (≈5%) of short gamma-ray bursts, which likely originate from NS–NS mergers, have physical (host-normalized) offsets comparable to or larger than the offset of FRB 20240209A (W.-f. Fong et al. 2022). Furthermore, only ≈10% of short gamma-ray burst host galaxies are quiescent (A. E. Nugent et al. 2022). Thus, while the environmental properties of FRB 20240209A are consistent

with a subset of kicked compact object binary progenitors, we find it to be a less plausible explanation.

6. Summary and Conclusion

The repeating FRB 20240209A was discovered by CHIME/FRB in 2024 February, with 22 repeat bursts detected up to 2024 July 31. The activity of this repeater evolved significantly over this period, with the source suddenly becoming very active in 2024 June. This indicates that FRB 20240209A also undergoes sudden episodes of increased activity, as has been seen in other repeaters. Additionally, the burst morphology of FRB 20240209A bursts is consistent with other repeaters.

The CHIME–KKO baseline provides a one-dimensional (1D) VLBI localization accuracy of $\sim 2''$ along the baseline vector for single pulse localizations. For the six repeat bursts recorded at KKO, the high decl. of FRB 20240209A allowed the bursts to be detected with a rotating range of baseline vectors, such that combining the multiple localizations constrained the localization region along several axes. This combined localization was inflated to account for correlated systematic errors, giving a final localization ellipse of dimensions $\sim 1'' \times 2''$.

We observed the field of FRB 20240209A with the Gemini-North telescope and obtained an image of depth $r \gtrsim 25.9$ mag. We use the VLBI localization and PATH to robustly associate FRB 20240209A with a luminous and quiescent elliptical galaxy at $z = 0.1384$ ($P(O|x) = 0.99$). This is the first association of a repeating FRB to a quiescent galaxy, and the first association of any FRB to an elliptical galaxy (see also T. Eftekhari et al. 2025). Moreover, the FRB has a projected physical offset of 40 ± 5 kpc from the center of the host galaxy, making it the most offset FRB host to date.

Given the large offset of the FRB from the host galaxy, we consider a progenitor that is either formed in situ or kicked from its birthplace. For the in situ case, an origin in a GC is possible with the projected offset of FRB 20240209A being consistent with the projected offsets of GCs in elliptical galaxies. Moreover, when normalized by the host galaxy size, the offset of FRB 20240209A is comparable to that of FRB 20200120E, providing further support for a GC origin. In such a scenario, promising progenitor models include magnetars formed via accretion-induced collapse of a WD, merger-induced collapse of a WD–WD, NS–WD, or NS–NS binary, LMXBs, or ULXs. An extreme scenario would be in situ formation in an undetected satellite dwarf galaxy of the putative host, which is $\gtrsim 10$ fainter than any other FRB host with known redshift. However, DM budgeting barely allows any DM from the host galaxy of the FRB at the redshift of the putative host, making a GC origin more favorable. For a kicked progenitor case, NS–NS or NS–WD mergers that produce stable neutron star remnants are a possibility, where the high kick velocities of these systems can explain the large offset. However, only a small fraction of short gamma-ray bursts, which are thought to be formed from kicked NS–NS mergers, are known to have similar or larger galactocentric offsets, or quiescent host galaxies. Thus, we consider in situ formation in a GC to be the more likely scenario.

We thus conclude that the unique local environment and host galaxy of FRB 20240209A revealed by its precise localization adds to the diversity of environments in which repeating FRBs are found. The precise localization of FRBs is crucial to understanding their origins. The CHIME–KKO localization of this repeater provides a proof of concept for the full three-station CHIME/FRB Outrigger array, which will be operational in the near future and which will enable subarcsecond localizations for thousands of FRBs to their local environments and host galaxies.

Acknowledgments

We acknowledge that CHIME and the k'niʔatn k'l⌣stk'masqt Outrigger (KKO) are built on the traditional, ancestral, and unceded territory of the Syilx Okanagan people. K'niʔatn k'l⌣stk'masqt is situated on land leased from the Imperial Metals Corporation. We are grateful to the staff of the Dominion Radio Astrophysical Observatory, which is operated by the National Research Council of Canada. CHIME operations are funded by a grant from the NSERC Alliance Program and by support from McGill University, the University of British Columbia, and the University of Toronto. CHIME/FRB Outriggers are funded by a grant from the Gordon & Betty Moore Foundation. We are grateful to Robert Kirshner for early support and encouragement of the CHIME/FRB Outriggers Project, and to Dusan Pejakovic of the Moore Foundation for continued support. CHIME was funded by a grant from the Canada Foundation for Innovation (CFI) 2012 Leading Edge Fund (Project 31170) and by contributions from the provinces of British Columbia, Québec, and Ontario. The CHIME/FRB Project was funded by a grant from the CFI 2015 Innovation Fund (Project 33213) and by contributions from the provinces of British Columbia and Québec, and by the Dunlap Institute for Astronomy and Astrophysics at the University of Toronto. Additional support was provided by the Canadian Institute for Advanced Research (CIFAR), the Trottier Space Institute at McGill University, and the University of British Columbia. The CHIME/FRB baseband recording system is funded in part by a CFI John R. Evans Leaders Fund award to IHS.

We are grateful to Jennifer Andrews and the Gemini Observatory staff for executing our Gemini observations. V. S. is supported by a Fonds de Recherche du Quebec—Nature et Technologies (FRQNT) Doctoral Research Award. K.S. is supported by the NSF Graduate Research Fellowship Program. C.L. is supported by NASA through the NASA Hubble Fellowship grant HST-HF2-51536.001-A awarded by the Space Telescope Science Institute, which is operated by the Association of Universities for Research in Astronomy, Inc., under NASA contract NAS5-26555. W.F. gratefully acknowledges support from the National Science Foundation under grant No. AST-2206494 and CAREER grant No. AST-2047919, the David and Lucile Packard Foundation, the Alfred P. Sloan Foundation, and the Research Corporation for Science Advancement through Cottrell Scholar Award #28284. T.E. is supported by NASA through the NASA Hubble Fellowship grant HST-HF2-51504.001-A awarded by the Space Telescope Science Institute, which is operated by the Association of Universities for Research in Astronomy, Inc., for NASA, under contract NAS5-26555.

B.C.A. is supported by a FRQNT Doctoral Research Award. M.B. is a McWilliams fellow and an International Astronomical Union Gruber fellow. M.B. also receives support from the McWilliams seed grant. A.C. is a Vanier Canada Graduate Scholar. M.D. is supported by a CRC Chair, NSERC Discovery Grant, CIFAR, and by the FRQNT Centre de Recherche en Astrophysique du Québec (CRAQ). Y.D. is

supported by the National Science Foundation Graduate Research Fellowship under grant No. DGE-2234667. F.A.D. is supported by the UBC Four Year Fellowship. E.F. and S.S.P. are supported by the National Science Foundation (NSF) grant AST-2407399. J.W.T.H. and the AstroFlash research group acknowledge support from a Canada Excellence Research Chair in Transient Astrophysics (CERC-2022-00009); the European Research Council (ERC) under the European Union's Horizon 2020 research and innovation program ("EuroFlash"; grant agreement No. 101098079); and an NWO-Vici grant ("AstroFlash"; VI.C.192.045). V.M.K. holds the Lorne Trottier Chair in Astrophysics & Cosmology, a Distinguished James McGill Professorship, and receives support from an NSERC Discovery grant (RGPIN 228738-13). K.W.M. holds the Adam J. Burgasser Chair in Astrophysics. K.N. is an MIT Kavli Fellow. A.P. is funded by the NSERC Canada Graduate Scholarships—Doctoral program. A.B.P. is a Banting Fellow, a McGill Space Institute (MSI) Fellow, and a FRQNT postdoctoral fellow. Z.P. is supported by an NWO Veni fellowship (VI.Veni.222.295). M. S. acknowledges support from the Trottier Space Institute Fellowship program. P.S. acknowledges the support of an NSERC Discovery grant (RGPIN-2024-06266). FRB research at UBC is supported by an NSERC Discovery Grant and by the Canadian Institute for Advanced Research.

Based on observations obtained at the international Gemini Observatory (Program ID: GN-2024A-LP-110), a program of NOIRLab, which is managed by the Association of Universities for Research in Astronomy (AURA) under a cooperative agreement with the National Science Foundation on behalf of the Gemini Observatory partnership: the National Science Foundation (United States), National Research Council (Canada), Agencia Nacional de Investigación y Desarrollo (Chile), Ministerio de Ciencia, Tecnologìa e Innovación (Argentina), Ministério da Ciência, Tecnologia, Inovações e Comunicações (Brazil), and Korea Astronomy and Space Science Institute (Republic of Korea).

This research has made use of the CIRADA cutout service at URL cutouts.cirada.ca, operated by the Canadian Initiative for Radio Astronomy Data Analysis (CIRADA). CIRADA is funded by a grant from the Canada Foundation for Innovation 2017 Innovation Fund (Project 35999), as well as by the Provinces of Ontario, British Columbia, Alberta, Manitoba, and Quebec, in collaboration with the National Research Council of Canada, the US National Radio Astronomy Observatory and Australia's Commonwealth Scientific and Industrial Research Organisation.

Facilities: CHIME, KKO, Gemini (GMOS).

Software: `Astropy` (Astropy Collaboration et al. 2013, 2018, 2022), `DM Phase` (A. Seymour et al. 2019), `fitburst` (E. Fonseca et al. 2024), `hdf5` (The HDF Group 1997-2023), `matplotlib` (J. D. Hunter 2007), `numpy` (C. R. Harris et al. 2020), `PyFX` (C. Leung et al. 2024).

Appendix A
Estimating the Burst Properties

For the bursts with baseband data, the data were beamformed to the best VLBI position of FRB 20240209A listed in Table 1. The baseband morphology pipeline uses the intensity (Stokes *I*) data in the beamformed file to fit a model with burst width, scattering, bandwidth, arrival time, and DM as parameters.

Table 2
Properties of the Repeat Bursts from FRB 20240209A

Burst	TNS Name	TOA	SNR	DM (pc cm^{-3})	Width (ms)	τ (ms)	t_{res} (ms)	Peak Flux (Jy)	Fluence (Jy ms)
B1*	FRB 20240209A	2024-02-09 07:10:14	15.99	176.49 ± 0.01	23.4	<0.2	0.082	20.9 ± 2.5	324.9 ± 33.4
B2	FRB 20240217A	2024-02-17 06:36:05	9.24	177.63 ± 0.24	29.7	<4.58	0.983	…	…
B3*	FRB 20240309A	2024-03-09 04:29:37	16.78	176.33 ± 0.03	1.9	<0.15	0.041	7.0 ± 0.8	12.9 ± 1.5
B4	FRB 20240608A	2024-06-08 10:23:09	9.0	175.4 ± 0.09	49.9	<2.99	0.983	…	…
B5	FRB 20240612A	2024-06-12 08:51:06	14.42	175.07 ± 0.14	32.1	<0.79	0.655	2.9 ± 0.6	18.2 ± 2.4
B6	FRB 20240612B	2024-06-12 21:33:20	10.89	176.82 ± 0.51	45.5	<19.32	0.983	…	…
B7	FRB 20240616A	2024-06-16 22:52:19	13.7	175.27 ± 0.04	3.8	<1.09	0.164	18.7 ± 2.7	64.9 ± 8.0
B8	FRB 20240619A	2024-06-19 08:57:36	10.46	175.12 ± 0.01	57.4	<0.72	0.328	3.9 ± 0.8	21.4 ± 2.6
B9	FRB 20240619B	2024-06-19 09:03:37	10.73	175.19 ± 0.02	17.7	<0.22	0.328	2.8 ± 0.5	21.2 ± 2.4
B10	FRB 20240619C	2024-06-19 10:11:00	10.3	176.51 ± 0.18	16.2	<6.88	0.983	…	…
B11	FRB 20240620A	2024-06-20 08:55:51	8.47	175.35 ± 0.14	55.5	<1.91	0.983	…	…
B12	FRB 20240620B	2024-06-20 09:14:46	8.53	175.91 ± 0.27	33.2	<4.02	0.983	…	…
B13	FRB 20240621A	2024-06-21 21:00:56	9.02	179.46 ± 0.77	63.2	<26.85	0.983	…	…
B14	FRB 20240625A	2024-06-25 20:20:30	12.29	175.39 ± 0.04	41.7	<1.27	0.983	…	…
B15	FRB 20240628A	2024-06-28 22:05:21	9.59	175.72 ± 0.16	30.5	<5.83	0.983	…	…
B16*	FRB 20240629A	2024-06-29 07:58:35	16.17	175.18 ± 0.01	16.4	<0.24	0.082	9.6 ± 1.1	113.7 ± 11.6
B17*	FRB 20240629B	2024-06-29 08:32:47	20.67	175.17 ± 0.01	15.6	<0.18	0.041	12.5 ± 1.4	46.5 ± 5.0
B18*	FRB 20240629C	2024-06-29 08:57:54	19.46	175.21 ± 0.04	2.7	<1.13	0.655	4.6 ± 0.8	7.4 ± 1.3
B19	FRB 20240629D	2024-06-29 11:07:02	9.7	176.47 ± 0.43	30.4	<12.93	0.983	…	…
B20*	FRB 20240629E	2024-06-29 19:16:34	16.12	175.37 ± 0.01	6.0	<0.44	0.164	30.1 ± 5.0	97.1 ± 13.1
B21	FRB 20240702A	2024-07-02 08:36:06	9.25	177.29 ± 0.3	20.9	<8.87	0.983	…	…
B22	FRB 20240716A	2024-07-16 06:14:15	8.6	175.3 ± 0.15	17.7	<7.5	0.983	…	…

Note. The burst number is used to refer to the individual bursts. * indicates the bursts detected at KKO and localized with the CHIME–KKO baseline. Although each burst has a different TNS name, all bursts are from the same repeating source FRB 20240209A, which has the TNS name of the first burst from this repeater. Topocentric TOAs are referenced at 400 MHz and calculated using the structure-maximizing DM indicated in the fifth column and a DM constant of $K_{DM} = 10^4/2.41$ s MHz^2 pc^{-1} cm^3. The scattering timescale τ is referenced at 600 MHz and reported as an upper limit equivalent to the width of the narrowest subburst. All burst properties are calculated at a time resolution t_{res}. Fluxes and fluences are not quoted for intensity bursts as our current pipelines can only estimate a lower limit on these values.

While the baseband data have a time resolution of 2.56 μs, the data are downsampled in time to achieve a higher SNR per sample for fitting. The pipeline has three main steps, as described by K. R. Sand et al. (2023, 2024). The first step involves radio frequency interference excision (D. Michilli et al. 2021), obtaining the structure-maximizing DM (J. W. T. Hessels et al. 2019) and dedispersion. The second step involves smoothing the burst profile and estimating the number of burst components. Then, the 1D time-series data and spectrum are fit to exponentially modified Gaussians (M. M. McKinnon 2014) and running power-law (CHIME/FRB Collaboration et al. 2021) models, respectively, where a Markov Chain Monte Carlo sampling algorithm is used to generate initial parameters for the next step. In the third step, the initial parameters are passed to `fitburst` (E. Fonseca et al. 2024) to perform a 2D least-square optimization fit on the dynamic spectrum of bursts and return the DM, time of arrival (TOA), signal amplitude, temporal width, power-law spectral index, spectral running, and scattering timescale (τ) of the bursts. The scattering time is assumed to go as $\tau \propto \nu^{-4}$ with frequency ν and with a reference frequency of 600 MHz. The burst properties for the bursts with intensity data were also estimated using `fitburst` and a similar procedure as described above. The only difference is the method to estimate the initial guesses for the fit parameters, which is described in CHIME/FRB Collaboration et al. (2021).

The fluxes and fluences for the baseband bursts were estimated using the procedure described in CHIME/FRB Collaboration et al. (2024) and the VLBI position of FRB 20240209A. The flux calibration pipeline for intensity bursts is set up to use the real-time localization of the burst estimated from the metadata stored during burst detection. Since the uncertainty on these "header" localizations can span several degrees, the pipeline can only estimate a lower limit on the flux and fluence (CHIME/FRB Collaboration et al. 2021; B. C. Andersen et al. 2023). We thus do not quote flux and fluence measurements for intensity bursts.

Table 2 lists the TOA, structure-maximizing DM, temporal width, and scattering time returned by `fitburst` for each of the 10 baseband bursts and 12 intensity bursts. The temporal width is the width of the FWHM of the burst envelope at 600 MHz. Since none of the bursts showed any obvious scattering visually, the scattering times are reported as upper limits, with the upper limit being the width of the narrowest subburst. Fluxes and fluences are listed for the 10 baseband bursts. Polarization analysis of the FRB 20240209A bursts will be presented in future works.

Appendix B
Systematic Error in CHIME–KKO Localizations

There can be multiple sources of systematic errors in the CHIME–KKO localizations. The residual ionospheric delays are expected to be a source of time-dependent systematic errors that are not correlated for data taken at different times. Another source of systematic error is the beam phase. The primary beam of each feed in the CHIME and KKO stations has an unknown phase that is not accounted for while obtaining geometric delays from the phase-calibrated visibilities (A. E. Lanman et al. 2024). The beam phase is expected to be time-independent and spatially dependent on the pointing of the correlator on the sky. Due to the high decl. of FRB 20240209A, the correlator pointing for each of the six repeat bursts is similar, and thus the systematic errors in the localizations due to the beam phase are correlated.

To obtain the correlated systematic error in the combined CHIME–KKO localization, we used 3–5 localizations from 12 pulsars each, which were obtained using the procedure described in Section 3 and by A. E. Lanman et al. (2024). For each localization, the calibrator that was closest to the pulsar on the sky and detectable within the same baseband dump as the pulsar pulse was used as the phase calibrator. Only the frequency channels used for FRB 20240209A localizations were used for the pulsar localizations, to remove any bandwidth dependence of errors. The multiple localizations were combined for each pulsar, and the offset of the combined localization position from the true pulsar position along the baseline vector was obtained. These "projected" offsets had an rms of $\sim 1''$. We assume that combining multiple localizations averaged down time-dependent errors, and thus the correlated systematic error in CHIME–KKO localizations is $\sim 1''$. While the conclusions of A. E. Lanman et al. (2024) tell us that the rms localization error in CHIME–KKO localizations for broadband one-off bursts is $\sim 1''$, the analysis here indicates that the rms error in combined localizations of narrowband bursts from repeaters is also $\sim 1''$.

Note that the beam phase error depends on the separation of the target and calibrator on the sky. The pulsar localizations had target-calibrator separations of tens of degrees, while the target-calibrator separation for FRB 20240209A is $\sim 4°$. We expect the beam phase error in the FRB 20240209A localizations to be similar for both the target and the calibrator since they are close together on the sky, and to be removed upon calibration. Thus, if the systematic error is dominated by the beam phase error, assuming a systematic error of $1''$ in the combined CHIME–KKO localization for FRB 20240209A gives us a conservative localization error.

ORCID iDs

Vishwangi Shah https://orcid.org/0000-0002-4823-1946
Kaitlyn Shin https://orcid.org/0000-0002-6823-2073
Calvin Leung https://orcid.org/0000-0002-4209-7408
Wen-fai Fong https://orcid.org/0000-0002-7374-935X
Tarraneh Eftekhari https://orcid.org/0000-0003-0307-9984
Mandana Amiri https://orcid.org/0000-0001-6523-9029
Bridget C. Andersen https://orcid.org/0000-0001-5908-3152
Shion Andrew https://orcid.org/0000-0002-3980-815X
Mohit Bhardwaj https://orcid.org/0000-0002-3615-3514
Charanjot Brar https://orcid.org/0000-0002-1800-8233
Tomas Cassanelli https://orcid.org/0000-0003-2047-5276
Shami Chatterjee https://orcid.org/0000-0002-2878-1502
Alice Curtin https://orcid.org/0000-0002-8376-1563
Matt Dobbs https://orcid.org/0000-0001-7166-6422
Yuxin Dong (董雨欣) https://orcid.org/0000-0002-9363-8606
Fengqiu Adam Dong https://orcid.org/0000-0003-4098-5222
Emmanuel Fonseca https://orcid.org/0000-0001-8384-5049
B. M. Gaensler https://orcid.org/0000-0002-3382-9558
Mark Halpern https://orcid.org/0000-0002-1760-0868
Jason W. T. Hessels https://orcid.org/0000-0003-2317-1446
Adaeze L. Ibik https://orcid.org/0000-0003-2405-2967
Naman Jain https://orcid.org/0009-0009-0938-1595
Ronniy C. Joseph https://orcid.org/0000-0003-3457-4670

Jane Kaczmarek https://orcid.org/0000-0003-4810-7803
Lordrick A. Kahinga https://orcid.org/0009-0007-5296-4046
Victoria M. Kaspi https://orcid.org/0000-0001-9345-0307
Bikash Kharel https://orcid.org/0009-0008-6166-1095
Tom Landecker https://orcid.org/0000-0003-1455-2546
Adam E. Lanman https://orcid.org/0000-0003-2116-3573
Mattias Lazda https://orcid.org/0000-0002-5857-4264
Robert Main https://orcid.org/0000-0002-7164-9507
Lluis Mas-Ribas https://orcid.org/0000-0003-4584-8841
Kiyoshi W. Masui https://orcid.org/0000-0002-4279-6946
Ryan Mckinven https://orcid.org/0000-0001-7348-6900
Juan Mena-Parra https://orcid.org/0000-0002-0772-9326
Bradley W. Meyers https://orcid.org/0000-0001-8845-1225
Daniele Michilli https://orcid.org/0000-0002-2551-7554
Kenzie Nimmo https://orcid.org/0000-0003-0510-0740
Ayush Pandhi https://orcid.org/0000-0002-8897-1973
Swarali Shivraj Patil https://orcid.org/0009-0008-7264-1778
Aaron B. Pearlman https://orcid.org/0000-0002-8912-0732
Ziggy Pleunis https://orcid.org/0000-0002-4795-697X
J. Xavier Prochaska https://orcid.org/0000-0002-7738-6875
Masoud Rafiei-Ravandi https://orcid.org/0000-0001-7694-6650
Mawson Sammons https://orcid.org/0000-0002-4623-5329
Ketan R. Sand https://orcid.org/0000-0003-3154-3676
Paul Scholz https://orcid.org/0000-0002-7374-7119
Kendrick Smith https://orcid.org/0000-0002-2088-3125
Ingrid Stairs https://orcid.org/0000-0001-9784-8670

References

Aggarwal, K., Budavári, T., Deller, A. T., et al. 2021, ApJ, 911, 95
Andersen, B. C., Patel, C., Brar, C., et al. 2023, AJ, 166, 138
Andrew, S., Leung, C., Li, A., et al. 2024, arXiv:2409.11476
Anna-Thomas, R., Connor, L., Dai, S., et al. 2023, Sci, 380, 599
Astropy Collaboration, Price-Whelan, A. M., Lim, P. L., et al. 2022, ApJ, 935, 167
Astropy Collaboration, Price-Whelan, A. M., Sipőcz, B. M., et al. 2018, AJ, 156, 123
Astropy Collaboration, Robitaille, T. P., Tollerud, E. J., et al. 2013, A&A, 558, A33
Bannister, K. W., Deller, A. T., Phillips, C., et al. 2019, Sci, 365, 565
Belczynski, K., Perna, R., Bulik, T., et al. 2006, ApJ, 648, 1110
Bethapudi, S., Spitler, L. G., Main, R. A., Li, D. Z., & Wharton, R. S. 2023, MNRAS, 524, 3303
Bhandari, S., Gordon, A. C., Scott, D. R., et al. 2023, ApJ, 948, 67
Bhandari, S., Heintz, K. E., Aggarwal, K., et al. 2022, AJ, 163, 69
Bhandari, S., Marcote, B., Sridhar, N., et al. 2023, ApJL, 958, L19
Bhandari, S., Sadler, E. M., Prochaska, J. X., et al. 2020, ApJL, 895, L37
Bhardwaj, M., Gaensler, B. M., Kaspi, V. M., et al. 2021, ApJL, 910, L18
Bhardwaj, M., Michilli, D., Kirichenko, A. Y., et al. 2024, ApJL, 971, L51
Bochenek, C. D., Ravi, V., Belov, K. V., et al. 2020, Natur, 587, 59
Bochenek, C. D., Ravi, V., & Dong, D. 2021, ApJL, 907, L31
Bruni, G., Piro, L., Yang, Y.-P., et al. 2024, Natur, 632, 1014
Cassanelli, T., Leung, C., Sanghavi, P., et al. 2024, NatAs, 8, 1429
Chatterjee, S., Law, C. J., Wharton, R. S., et al. 2017, Natur, 541, 58
CHIME Collaboration, Amiri, M., Bandura, K., et al. 2022, ApJS, 261, 29
CHIME/FRB Collaboration, Amiri, M., Bandura, K., et al. 2018, ApJ, 863, 48
CHIME/FRB Collaboration, Amiri, M., Andersen, B. C., et al. 2020a, Natur, 582, 351
CHIME/FRB Collaboration, Amiri, M., Andersen, B. C., et al. 2021, ApJS, 257, 59
CHIME/FRB Collaboration, Amiri, M., Andersen, B. C., et al. 2024, ApJ, 969, 145
CHIME/FRB Collaboration, Andersen, B. C., Bandura, K. M., et al. 2020b, Natur, 587, 54
CHIME/FRB Collaboration, Andersen, B. C., Bandura, K., et al. 2023, ApJ, 947, 83
Clark, G. W. 1975, ApJL, 199, L143
Connor, L., Ravi, V., Sharma, K., et al. 2024, arXiv:2409.16952
Cook, A. M., Bhardwaj, M., Gaensler, B. M., et al. 2023, ApJ, 946, 58
Cordes, J. M., & Lazio, T. J. W. 2002, arXiv:astro-ph/0207156
Dage, K. C., Kundu, A., Thygesen, E., et al. 2021, MNRAS, 504, 1545
Dong, Y., Eftekhari, T., Fong, W.-f., et al. 2024, ApJ, 961, 44
Eftekhari, T., & Berger, E. 2017, ApJ, 849, 162
Eftekhari, T., Dong, Y., Fong, W., et al. 2025, ApJL, 979, L23
Fong, W.-f., Nugent, A. E., Dong, Y., et al. 2022, ApJ, 940, 56
Fonseca, E., Andersen, B. C., Bhardwaj, M., et al. 2020, ApJL, 891, L6
Fonseca, E., Pleunis, Z., Breitman, D., et al. 2024, ApJS, 271, 49
Gajjar, V., Siemion, A. P. V., Price, D. C., et al. 2018, ApJ, 863, 2
Geminardi, A., Pelliciari, D., Esposito, P., et al. 2024, ATel, 16692, 1
Gordon, A. C., Fong, W.-f., Kilpatrick, C. D., et al. 2023, ApJ, 954, 80
Harris, C. R., Millman, K. J., van der Walt, S. J., et al. 2020, Natur, 585, 357
Harris, W. E. 1996, AJ, 112, 1487
Heintz, K. E., Prochaska, J. X., Simha, S., et al. 2020, ApJ, 903, 152
Hessels, J. W. T., Spitler, L. G., Seymour, A. D., et al. 2019, ApJL, 876, L23
Hewitt, D. M., Bhandari, S., Marcote, B., et al. 2024a, MNRAS, 529, 1814
Hewitt, D. M., Bhardwaj, M., Gordon, A. C., et al. 2024b, ApJL, 977, L4
Hewitt, D. M., Hessels, J. W. T., Ould-Boukattine, O. S., et al. 2023, MNRAS, 526, 2039
Hunter, J. D. 2007, CSE, 9, 90
Ibik, A. L., Drout, M. R., Gaensler, B. M., et al. 2024a, ApJ, 961, 99
Ibik, A. L., Drout, M. R., Gaensler, B. M., et al. 2024b, ApJ, 976, 199
James, C. W. 2023, PASA, 40, e057
Josephy, A., Chawla, P., Fonseca, E., et al. 2019, ApJL, 882, L18
Kirsten, F., Marcote, B., Nimmo, K., et al. 2022, Natur, 602, 585
Kremer, K., Piro, A. L., & Li, D. 2021, ApJL, 917, L11
Lacy, M., Baum, S. A., Chandler, C. J., et al. 2020, PASP, 132, 035001
Lanman, A. E., Andersen, B. C., Chawla, P., et al. 2022, ApJ, 927, 59
Lanman, A. E., Andrew, S., Lazda, M., et al. 2024, AJ, 168, 87
Law, C. J., Bhardwaj, M., Burke-Spolaor, S., et al. 2024, ATel, 16701, 1
Law, C. J., Sharma, K., Ravi, V., et al. 2024c, ApJ, 967, 29
Lee-Waddell, K., James, C. W., Ryder, S. D., et al. 2023, PASA, 40, e029
Leung, C., Andrew, S., Masui, K. W., et al. 2024, arXiv:2403.05631
Leung, C., Mena-Parra, J., Masui, K., et al. 2021, AJ, 161, 81
Li, D., Wang, P., Zhu, W. W., et al. 2021, Natur, 598, 267
Lian, J., Zasowski, G., Chen, B., et al. 2024, NatAs, 8, 1302
Lu, W., & Kumar, P. 2018, MNRAS, 477, 2470
Lu, W., Kumar, P., & Zhang, B. 2020, MNRAS, 498, 1397
Maccarone, T. J., Kundu, A., Zepf, S. E., & Rhode, K. L. 2007, Natur, 445, 183
Majid, W. A., Pearlman, A. B., Prince, T. A., et al. 2021, ApJL, 919, L6
Mannings, A. G., Fong, W.-f., Simha, S., et al. 2021, ApJ, 917, 75
Marcote, B., Nimmo, K., Hessels, J. W. T., et al. 2020, Natur, 577, 190
Marcote, B., Paragi, Z., Hessels, J. W. T., et al. 2017, ApJL, 834, L8
Margalit, B., & Metzger, B. D. 2019, ApJL, 880, L15
McKinnon, M. M. 2014, PASP, 126, 476
McKinven, R. & CHIME/FRB Collaboration 2022, ATel, 15679, 1
Mena-Parra, J., Leung, C., Cary, S., et al. 2022, AJ, 163, 48
Metzger, B. D., Margalit, B., & Sironi, L. 2019, MNRAS, 485, 4091
Michilli, D., Bhardwaj, M., Brar, C., et al. 2023, ApJ, 950, 134
Michilli, D., Masui, K. W., Mckinven, R., et al. 2021, ApJ, 910, 147
Michilli, D., Seymour, A., Hessels, J. W. T., et al. 2018, Natur, 553, 182
Nantais, J. B., & Huchra, J. P. 2010, AJ, 139, 2620
Nantais, J. B., Huchra, J. P., McLeod, B., Strader, J., & Brodie, J. P. 2010, AJ, 139, 1413
Nimmo, K., Hessels, J. W. T., Keimpema, A., et al. 2021, NatAs, 5, 594
Nimmo, K., Hessels, J. W. T., Kirsten, F., et al. 2022a, NatAs, 6, 393
Nimmo, K., Hessels, J. W. T., Snelders, M. P., et al. 2023, MNRAS, 520, 2281
Nimmo, K., Hewitt, D. M., Hessels, J. W. T., et al. 2022b, ApJL, 927, L3
Niu, C. H., Aggarwal, K., Li, D., et al. 2022, Natur, 606, 873
Nugent, A. E., Fong, W.-F., Dong, Y., et al. 2022, ApJ, 940, 57
Ocker, S. K., & Cordes, J. M. 2024, RNAAS, 8, 17
Ould-Boukattine, O. S., Hessels, J. W. T., Snelders, M. P., et al. 2024, ATel, 16732, 1
Pearlman, A. B. 2024, in United States National Committee of URSI National Radio Science Meeting (USNC-URSI NRSM) (Boulder, CO: IEEE), 1
Pearlman, A. B., Scholz, P., Bethapudi, S., et al. 2024, NatAs, Advanced Online Publication
Pellegrini, S., Siemiginowska, A., Fabbiano, G., et al. 2007, ApJ, 667, 749
Petroff, E., Hessels, J. W. T., & Lorimer, D. R. 2022, A&ARv, 30, 2
Planck Collaboration, Aghanim, N., Akrami, Y., et al. 2020, A&A, 641, A6
Platts, E., Weltman, A., Walters, A., et al. 2019, PhR, 821, 1
Pleunis, Z., Good, D. C., Kaspi, V. M., et al. 2021a, ApJ, 923, 1
Pleunis, Z., Michilli, D., Bassa, C. G., et al. 2021b, ApJL, 911, L3

Prochaska, J. X., & Zheng, Y. 2019, MNRAS, 485, 648
Rajwade, K. M., Bezuidenhout, M. C., Caleb, M., et al. 2022, MNRAS, 514, 1961
Ravi, V., Catha, M., D'Addario, L., et al. 2019, Natur, 572, 352
Rogers, A. E. E. 1970, RaSc, 5, 1239
Sand, K. R., Breitman, D., Michilli, D., et al. 2023, ApJ, 956, 23
Sand, K. R., Curtin, A. P., Michilli, D., et al. 2024, arXiv:2408.13215
Sanghavi, P., Leung, C., Bandura, K., et al. 2023, arXiv:2304.10534
Seymour, A., Michilli, D., & Pleunis, Z., 2019 DM_phase: Algorithm for Correcting Dispersion of Radio Signals, Astrophysics Source Code Library, ascl:1910.004
Shah, V. & CHIME/FRB Collaboration 2024, ATel, 16670, 1
Shannon, R. M., Bannister, K. W., Bera, A., et al. 2024, arXiv:2408.02083
Sharma, K., Ravi, V., Connor, L., et al. 2024, Natur, 635, 61
Sharma, K., Somalwar, J., Law, C., et al. 2023, ApJ, 950, 175
Sheth, K., Regan, M., Hinz, J. L., et al. 2010, PASP, 122, 1397
Shin, K., Masui, K. W., Bhardwaj, M., et al. 2023, ApJ, 944, 105
Snelders, M. P., Nimmo, K., Hessels, J. W. T., et al. 2023, NatAs, 7, 1486
Spitler, L. R., Forbes, D. A., Strader, J., Brodie, J. P., & Gallagher, J. S. 2008, MNRAS, 385, 361
Sridhar, N., Metzger, B. D., Beniamini, P., et al. 2021, ApJ, 917, 13
Strader, J., Brodie, J. P., Spitler, L., & Beasley, M. A. 2006, AJ, 132, 2333
Tendulkar, S. P., Bassa, C. G., Cordes, J. M., et al. 2017, ApJL, 834, L7
The HDF Group 1997–2023, Hierarchical Data Format, v5
Usher, C., Forbes, D. A., Spitler, L. R., et al. 2013, MNRAS, 436, 1172
Woodland, M. N., Mannings, A. G., Prochaska, J. X., et al. 2024, ApJ, 973, 64
Yamasaki, S., & Totani, T. 2020, ApJ, 888, 105
Yao, J. M., Manchester, R. N., & Wang, N. 2017, ApJ, 835, 29
Zhang, J., Wu, Q., Cao, S., et al. 2024, ATel, 16505, 1
Zhang, Y.-K., Li, D., Zhang, B., et al. 2023, ApJ, 955, 142
Zhang, Y.-K., Wang, P., Feng, Y., et al. 2022, RAA, 22, 124002